Journal of Pharmaceutical Investigation (2022) 52:243–257
https://doi.org/10.1007/s40005-022-00559-x

Online ISSN 2093-6214
Print ISSN 2093-5552

ORIGINAL ARTICLE

Active targeting via ligand-anchored pH-responsive strontium nanoparticles for efficient nucleic acid delivery into breast cancer cells

Athirah Bakhtiar[1] · Qing Xin Liew[2] · Khuen Yen Ng[1] · Ezharul Hoque Chowdhury[3]

Received: 6 October 2021 / Accepted: 13 January 2022 / Published online: 25 January 2022

Abstract

Purpose Gene therapy is a promising and novel therapeutic strategy for many mutated gene-associated diseases, including breast cancer. However, it poses significant biological drawbacks such as rapid clearance from the circulatory system and low cellular uptake of the exogenously delivered functional nucleic acids. The development of efficient and biocompatible carriers for genetic materials has been extensively explored in the literature, and the functionalization of nanoparticles (NPs) with cancer cell-recognizing ligands has become an attractive approach to promote tumor targetability and efficient cellular internalization via endocytosis.

Methods This study introduced self-assembling targeting ligands, including transferrin and fibronectin with the ability to electrostatically interact with strontium nanoparticles (SNPs), and then analyzed their influence on size and zeta potential of the resultant hybrid SNPs, cellular uptake and expression efficiency of transgene-loaded hybrid NPs.

Results Smaller ligand-coated SNPs (LCSNPs) remarkably increased gene transfection activity in both MCF-7 and 4T1 cells as well as nucleic acid localization into tumor tissues with improved tumor regression activity in a 4T1-tumor xenograft mouse model.

Conclusion LCSNPs-mediated delivery of p53 gene and MAPK siRNA provided a proof-of-concept for the functionalized nanocarrier formulation in order to inhibit breast cancer cell growth.

Keywords Transferrin · Fibronectin · Inorganic nanoparticles · Breast cancer · Gene therapy

Introduction

Gene therapy is an attractive approach for diseases with single or multiple gene defects such as breast cancer. The strategy that involves the introduction of genes into the targeted pathological cells alters the expression of the endogenous gene, aiming to treat or inhibit the disease progression (Chen et al. 2016; Montaño-Samaniego et al. 2020). However, naked nucleic acids are inefficiently internalized by target cells, primarily due to serum nuclease susceptibility and rapid biological clearance, besides low cellular uptake associated with negatively charged glucosaminoglycan chains of syndecan that repel intracellular entry of negatively-charged genetic materials (Durymanov and Reineke 2018). Various types of gene vectors were developed and studied to overcome the extracellular and intracellular barriers, namely viral and non-viral vectors. Despite effective gene transportation demonstrated by viral vectors, high immunogenicity, oncogenicity, limited DNA loading capacity, and expensive production limit their use, promoting the development of many non-viral carriers (Ramamoorth and Narvekar 2015). However, existing non-viral vectors are much more inefficient compared to their viral counterparts. We have recently established pH-responsive strontium nanoparticles (SNPs) with proficient gene binding and cellular uptake activity, enabling apoptosis induction in human and murine mammary cancer cells following delivery of p53 gene and MAPK siRNA in vitro

✉ Athirah Bakhtiar
athirah.bakhtiar@monash.edu

✉ Ezharul Hoque Chowdhury
md.ezharul.hoque@monash.edu

[1] School of Pharmacy, Monash University Malaysia, 47500 Bandar Sunway, Selangor, Malaysia

[2] Faculty of Pharmacy, MAHSA University, 42150 Jenjarom, Selangor, Malaysia

[3] Jeffrey Cheah School of Medicine and Health Sciences, Monash University Malaysia, Jalan Lagoon Selatan, 47500 Bandar Sunway, Selangor, Malaysia

and in vivo (Bakhtiar and Chowdhury 2021; Bakhtiar et al. 2021). Nevertheless, SNPs are associated with major biological downside associated with high tissue sequestration and low blood circulation time, largely affecting intracellular gene transport and expression. Opsonins, which might have a binding affinity to the SNPs, are likely to be responsible for eliminating the nanoparticles (NPs) via the reticuloendothelial system (RES) from the blood circulation, resulting in high depositions in the RES organs, such as kidneys and liver with lower accumulation in tumor site (Bakhtiar et al. 2021; Yu and Zheng 2015).

Conjugation of the ligands with the surface of nanovehicle, an approach known as active targeting, incorporates unique ligands that bind exclusively to the target receptors that are highly expressed in the cancer cells (Rosenblum et al. 2018). Overexpression of receptors or antigens in mammary carcinoma cells enables robust ligand-receptor recognition and adhesion for subsequent cellular uptake via receptor-mediated endocytosis (Deshpande et al. 2013). There are a few highly unique targets, such as transferrin (Tf) and fibronectin (Fb) that are overexpressed in many cancers including breast carcinoma. Tf receptor (TfR) was found to be highly concentrated in the cell membrane of mammary carcinoma cells and endothelial cells of the brain. The tfR-lytic peptide was actively targeted towards the cancerous cells with less toxicity observed in normally dividing cells (Daniels et al. 2012). It is apparent that TfR, an iron-binding glycoprotein, is overexpressed in carcinoma cells to facilitate the internalization of iron that is necessary for tumorigenesis and tumor growth (Shen et al. 2018; Candelaria et al. 2021). Fb is a ubiquitous glycoprotein that facilitates the estrogen activity in breast cancer cells to promote the proliferation of the mammary carcinoma cells (Wang and Hielscher 2017). Fb is often present in the tumor extracellular matrix surrounding the cancerous tissues, especially in early metastasis. Fb also prevents carcinoma cells from lysosomal degradation, resulting in the development of resistance towards hormonal therapy (Lin et al. 2019; Sampayo et al. 2018). Strategizing the advantages of NPs and overexpressed receptors as docking sites for cancer cells showed a notable role in enhancing antitumor activity of solid cancers including breast, brain, and pancreatic carcinoma (Rosenblum et al. 2018; Bazak et al. 2015).

We developed a facile method to fabricate ligand-associated nanocarrier to enhance the gene delivery of SNPs via electrostatically complexing Tf or Fb protein with the particle surfaces. Their ability to influence the structural characteristics of SNPs was investigated, notably on the average particle size and surface charge. Subsequently, transfection activity and anti-cancer effects of pDNA- or siRNA-loaded, ligand-anchored complexes were assessed in MCF-7 and 4T1 mammary cancer cells as well as in murine mammary tumor models.

Materials and methods

Materials

Dulbecco's modified Eagle's medium (DMEM), fetal bovine serum (FBS), penicillin, neomycin, streptomycin, and MTT [3-(4,5-dimethylthiazol-2-yl)-2,5-diphenyltetrazolium bromide] were purchased from Gibco BRL (Tennessee, USA). Sodium fluoride (NaF), sodium sulfite (Na_2SO_3), strontium chloride ($SrCl_2$), calcium chloride ($CaCl_2$), sodium bicarbonate (Na_2CO_3), 4-(2-hydroxyethyl)-1-piperazineethanesulfonic acid (HEPES)-buffered media, dimethyl sulfoxide (DMSO), fibronectin protein (rat plasma) (Fb) and transferrin (rat plasma) (Tf) were from Sigma-Aldrich (Missouri, USA). The pGL3-control encoding firefly luciferase and Steady-GloTM Luciferase Assay System were obtained from Promega (Madison, USA). The recombinant pCEP4 vector containing wild-type p53 (wt-human p53 cDNA), plasmid DNA (pDNA) with cytomegalovirus promoter, and enhanced green fluorescent protein (eGFP) and reporter gene (pCMV-eGFP,4.7 kb) were from Addgene. AF 488 siRNA (fluorescence siRNA) was bought from Qiagen (Hilden, Germany).

Cell culture and seeding

Human mammary carcinoma cells, MCF-7, and murine mammary carcinoma cell, 4T1, were from the American Type Culture Collection (ATCC, Manassas, USA). The cells were cultured in 75 cm^2 flasks in DMEM supplemented with 10% FBS, 50 µg penicillin/ml, 100 µg neomycin/ml, and 50 µg streptomycin/ml. The environmental condition was habituated at 37 °C in a humidified 5% CO_2-containing atmosphere. Sub-culturing was executed following trypsinization of the adherent cells and detached cells were shifted into appropriate numbers to a new plate with 10% serum-supplemented DMEM upon 90% confluency. All breast cancer cells at the exponential growth phase were seeded at 50,000 cells per well into 24-well plates before treatment.

4T1 cells-derived xenografts

The 4T1 tumor cells (50,000 cells/mouse) were subcutaneously inoculated into the mammary glands of 6–8-week-old BALB/c mice before being assigned to the random grouping of six mice/group (day 1). Each group of mice were housed in clean polypropylene cages and provided with a commercial pellet diet and water with a 12 h light/dark cycle. The animal study was conducted following the institutional ethics committee regulations on animal welfare (Monash University Animal Ethics no: MARP/2012/087). Tumor growth

was observed daily using a vernier caliper and allowed to grow to approximately 100 mm^3 (–day 14) before initiation of treatment.

Preparation of plasmid DNA (pDNA)

The transformation and propagation of pDNA were done using standard microbiological techniques. Briefly, HT5 α line *E. coli* containing pDNA was inoculated in LB broth and grown at 37 °C and 270 RPM overnight. pDNA was isolated from the bacteria using Qiagen EndoFree Plasmid Mega Kit (Hilden, Germany) as per the manufacturer's protocol. The concentration and quality of pDNA were determined using a DNA/RNA calculator (GeneQuant, USA).

Synthesis and characterization of ligand-conjugated strontium nanoparticles (LCSNPs)

Preparation commenced with the mixing of 2 µl of 1 M Na_2SO_3 or NaF with 5 µl of 1 M $SrCl_2$ to generate strontium sulfite ($SrSO_3$) or strontium fluoride (SrF_2), respectively, in 5 µl of HEPES-buffered media (pH 7.4) through incubation at 37 °C for 30 min. 1 µg of Fb or Tf was subsequently added into the generated particles and incubated for 10 min at 37 °C. FBS-supplemented DMEM was incorporated to obtain a 1 ml solution. Carbonate apatite (CO_3 AP) as a positive control was prepared by mixing the exogenous 5 mM $CaCl_2$ with 900 µl bicarbonate-buffered DMEM (pH 7.4) and incubating for 10 min at 37 °C. Fb or Tf weighed 1 µg was subsequently added, followed by an additional incubation at 37 °C for 10 min and addition of 10% FBS to similarly attain a 1 ml solution. Turbidity measurement was done using a UV–Visible spectrophotometer (UV-1800 Shimadzu, Japan). The spectrophotometric measurement was performed in triplicates and data analysis included the mean ± SD.

The size and morphology of particles were visualized using an optical microscope (Olympus, Japan) and a field emission-scanning electron microscope (FE-SEM) (Hitachi, Japan). The prepared samples were centrifuged at 15,000 RPM for 10 s, before removal of supernatant and resuspension with milli-Q water. Samples were maintained on ice to prevent particle growth before microscopic observation. A volume of 1 µl from each sample was positioned on a carbon tape-coated sample holder and dried at room temperature, followed by platinum sputtering of the samples for 30 s. Images of sputtered SNPs were captured at 10–15 kV. Measurement of average size, zeta potential, and polydispersity of LCSNPs was acquired via ZetaSizer (Malvern, Nano ZS UK) using a special capillary cuvette. A refractive index (RI) ratio of 1.325 (measured using DMEM with a refractometer) was used. The analysis was carried out using a ZetaSizer software 6.20 and all samples were represented as mean ± SD.

Dissolution of LCSNPs in acidic environment (for pH-responsive activity) was performed through addition of 1 M hydrochloric acid (HCl) into the generated SNPs to observe changes in turbidity as a result of a gradual decline in pH from 7.5 to 6.5, 5.5, 4.5 and 3.5, mimicking the changes in pH within the endosomal cavity following endocytosis. The influence of pH adjustment towards particles were monitored via turbidity changes at absorbance of 320 nm wavelength. The activity was conducted in triplicates, expressed as mean ± SD.

Cellular uptake analysis of LCSNPs

MCF-7 cells from the exponential growth phase were seeded at 50,000 cells per well into 24-well plates a day before transfection. pGFP of 1 µg or 10 nM AF488 siRNA was introduced into 5 µl of 1 M $SrCl_2$ in 10 µl HEPES-buffered solution, followed by supplementation of 2 µl of 1 M Na_2SO_3 or NaF and incubation at 37 °C for 30 min. Fb or Tf of 1 µg was subsequently added and incubated for 10 min. FBS-supplemented DMEM was incorporated to obtain the 1 ml solution. LCSNPs were inoculated with seeded carcinoma cells for 4 h, followed by removal of media, washing with 10 mM EDTA in PBS, and addition of 100 µl of DMEM. Fluorescence intensity was measured using a fluorescence microscope (Olympus, Japan) equipped with the FITC filter.

In vitro gene transfection with LCSNPs

pGL3 of 1 µg was incorporated into 5 µl of 1 M $SrCl_2$ and 2 µl of 1 M of NA_2SO_3 or NaF in 10 µl HEPES, followed by incubation at 37 °C for 30 min. Fb or Tf was subsequently added before incubation for 10 min at 37 °C and addition of DMEM to achieve 1 ml particle suspension. Plasmid-loaded LCSNPs were used to transfect MCF-7 or 4T1 cells for 4 h, followed by replacement of media with 1 ml of complete media after washing with EDTA in 1X PBS. The transfected cells were incubated for 48 h before quantitation of luciferase expression using a commercial kit and photon counting. The cells were lysed and centrifuged, followed by isolation of supernatant from the lysate to determine intracellular luminescence activity. Analysis was conducted in triplicates and expressed in a graph as mean ± SD of luminescence intensity/mg of protein.

To assess the fraction of viable cells, the 3-(4,5-dimethylthiazol-2-yl)-2,5-diphenyl-2H-tetrazolium bromide (MTT) assay was conducted following incubation of the transfected cells for 24, 48, and 72 h. MCF-7 and 4T1 cells were treated with LCSNPs complexed with 1 µg p53 plasmid or 10 nM MAPK siRNA. CO_3 AP and untreated cells were used as positive and negative controls, respectively. A volume of

50 µl of MTT (5 mg/ml in PBS) was briefly added to the treated cells, followed by incubation at 37 °C and 5% CO_2 for 4 h. A medium containing MTT was aspirated, and the formazan crystals formed at the bottom of each well were dissolved by the addition of 300 µl DMSO. The absorbance of the resultant solution was determined at 595 nm wavelength using a microplate reader (Dynex Opsys MR, USA) with a reference *t* wavelength of 630 nm. Each experiment was completed in triplicates and expressed in a graph as mean ± SD. Cell viability was calculated as follows:

$$\%\ \text{of cell viability (CV)} = \frac{OD_{\text{treated}} - OD_{\text{reference}}}{OD_{\text{untreated}} - OD_{\text{reference}}} \times 100\%$$

Analysis of MAPK and AKT pathway following intracellular delivery of MAPK siRNA

MAPK-siRNA-treated cells (in Sect. Cellular uptake analysis of LCSNPs) were lysed with IP Lysis Buffer and subjected to centrifugation process at 13,000 RPM at 4 °C for 20 min. A volume of 5 µl from the supernatant containing protein sample was aspirated to estimate the total amount of proteins via bovine serum albumin (BSA) assay kit (instruction based on manufacturer's manual). BSA protein was used to acquire the standard curve to measure total protein concentration from cellular lysates, based on the absorbance intensity. The remaining samples were aliquoted and stored at −80 °C before analysis on SDS-PAGE and Western blot. A volume of 10 µl of 10X loading dye was mixed with the cellular lysates containing 30 µg of total protein and subjected to SDS-PAGE using stain-free mini protein SFX gels (15 wells) in 1X running buffer at 0.01 amp/gel. The precision plus protein standards dual-color of 7 µl was used as a molecular weight marker to determine the molecular weight of the sampled proteins. The transfer of protein samples from gel to the 0.2 µm polyvinylidene fluoride (PVDF) membranes attached to trans-blot turbo transfer pack via trans-blot turbo transfer system was completed in 7 min at 1.3 amp, followed by blocking in in 1X TBST containing 5% skimmed milk for 1 h at room temperature. The membrane was subsequently incubated with primary antibodies (pMAPK, TMAPK, pAKT, TAKT, and GAPDH as loading reference) at 4 °C overnight with mild agitation, followed by washing in 1X TBST for 5 times to remove unbound primary antibodies (Table 1). HRP-conjugated goat anti-rabbit secondary antibody, Ig G (1:3000) was introduced into the membrane and incubated for 1 h with a gentle shake before washing for 5 times in 1X TBST to eliminate the unbound antibodies. The membrane was incubated with enhanced chemiluminescence (ECL) mixture for 5 min before the observation of bands using the XRS Chemidoc system.

Tissue biodistribution of LCSNPs

A 1 µM AF 488 siRNA was added into 5 µl of 1 M $SrCl_2$ and 2 µl of 1 M of Na_2SO_3 or NaF in HEPES-buffered media, followed by incubation for 30 min at 37 °C to fabricate the respective particles and addition of DMEM to obtain 100 µl solution (Table 2). Tf or Fb of 1 µg was incorporated into the formulated particles before incubation for 10 min at 37 °C. Following centrifugation and removal of the supernatant, LCSNPs were intravenously introduced into the mice's caudal tail vein. After 4 h, the mice were sacrificed, and the tissues of the brain, kidneys, liver, lung, spleen, and tumor were harvested, washed with 1X chilled PBS, and maintained on ice. 1 ml of chilled lysis buffer per 500 g of the harvested organ tissues was subsequently added and the tissues were homogenized using Omni Tissue Homogenizer (Omni, USA), before centrifugation at 4 °C for 10 min at 15,000 RPM.

The centrifuged supernatant in 100 µl volume was added into a 96-well black Opti-plate for fluorescence intensity measurement of AF 488-labeled siRNA. 2030 multilabel reader Victor TM X5 (Perkin Elmer, USA) with Perkin Elmer 2030 manager software was used to determine the intensity at $\lambda_{ex} = 490$ nm and $\lambda_{em} = 535$ nm. The data were represented as mean ± SD of fluorescence intensity/500 mg of organ mass.

Tumor regression activity of LCSNPs

SNPs in 100 µl volume loaded with 20 µg of p53 plasmid or 50 mM MAPK siRNA was administered via the mouse's caudal tail vein (described in Table 3). The treatment was repeated for two days following the first inoculation. The

Table 1 Antibodies for western blot analysis

Name	Company	Molecular weight	Clonality	Antibody dilution
P-p44/42 MAPK	Cell signaling	44 kDa 42 kDa	Monoclonal	1:2000
p44/42 MAPK	Cell signaling	44 kDa 42 kDa	Monoclonal	1:1000
P-Akt (Ser473)	Cell signaling	60 kDa	Monoclonal	1:2000
Akt (pan)	Cell signaling	60 kDa	Monoclonal	1:1000
GAPDH	Cell signaling	37 kDa	Monoclonal	1:3000

Table 2 The grouping for siRNA biodistribution study

Salt	Regimen
	A volume of 5 µl of 1 M $SrCl_2$ in 10 µl HEPES media; 2 µl of 1 M Na_2SO_3 added into the mixture, followed by DMEM-10% FBS to make up a 100 µl solution
$SrSO_3$	A volume of 5 µl of 1 M $SrCl_2$ in 10 µl HEPES media; 2 µl of 1 M Na_2SO_3 added into the mixture, followed by 1 µg of Tf. DMEM-10% FBS was incorporated to obtain a 100 µl solution
	A volume of 5 µl of 1 M $SrCl_2$ in 10 µl HEPES media; 2 µl of 1 M Na_2SO_3 added into the mixture, followed by 1 µg of Fb. DMEM-10% FBS was incorporated to obtain a 100 µl solution
	A volume of 5 µl of 1 M $SrCl_2$ in 10 µl HEPES media; 2 µl of 1 M NaF added into the mixture, followed by DMEM-10% FBS to achieve a 100 µl solution
SrF_2	A volume of 5 µl of 1 M $SrCl_2$ in 10 µl HEPES media; 2 µl of 1 M NaF added into the mixture, followed by 1 µg of Tf. DMEM-10% FBS was incorporated to obtain a 100 µl solution
	A volume of 5 µl of 1 M $SrCl_2$ in 10 µl HEPES media; 2 µl of 1 M NaF added into the mixture, followed by 1 µg of Fb. DMEM-10% FBS was incorporated to obtain a 100 µl solution
	A 44 mM Na_2CO_3 and 5 mM $CaCl_2$ were added to DMEM-10% FBS to achieve a final volume of 100 µl
CO_3 AP	A 44 mM Na_2CO_3 and 5 mM $CaCl_2$ were added to DMEM-10% FBS to achieve a final volume of 100 µl with 1 µg of Tf
	A 44 mM Na_2CO_3 and 5 mM $CaCl_2$ were added to DMEM-10% FBS to achieve a final volume of 100 µl with 1 µg of Fb
Untreated	A volume of 100 µl of PBS

Table 3 The grouping for tumor regression study

Group	Regimen
	p53 of 20 µg or 50 mM MAPK siRNA was incorporated into a 5 µl of 1 M $SrCl_2$ in 10 µl HEPES media; 2 µl of 1 M Na_2SO_3 was added into the mixture, followed by DMEM-10% FBS to achieve a final volume of 100 µl
$SrSO_3$	p53 of 20 µg or 50 mM MAPK siRNA was incorporated into a 5 µl of 1 M $SrCl_2$ in 10 µl HEPES media; 2 µl of 1 M Na_2SO_3 was added into the mixture, followed by 1 µg of Tf. DMEM-10%cFBS was incorporated to obtain a final volume of 100 µl
	p53 of 20 µg or 50 mM MAPK siRNA was incorporated into a 5 µl of 1 M $SrCl_2$ in 10 µl HEPES media; 2 µl of 1 M Na_2SO_3 added into the mixture, followed by 1 µg of Fb. DMEM-10% FBS was incorporated to obtain a final volume of 100 µl
	p53 of 20 µg or 50 mM MAPK siRNA was incorporated into a 5 µl of 1 M $SrCl_2$ in 10 µl HEPES media; 2 µl of 1 M NaF added into the mixture, followed by DMEM-10% FBS to achieve a final volume of 100 µl
SrF_2	p53 of 20 µg or 50 mM MAPK siRNA was incorporated into a 5 µl of 1 M $SrCl_2$ in 10 µl HEPES media; 2 µl of 1 M NaF added into the mixture, followed by 1 µg of Tf. DMEM-10% FBS was incorporated to obtain a final volume of 100 µl
	p53 of 20 µg or 50 mM MAPK siRNA was incorporated into a 5 µl of 1 M $SrCl_2$ in 10 µl HEPES media; 2 µl of 1 M NaF was added into the mixture, followed by 1 µg of Fb. DMEM-10% FBS was incorporated to obtain a final volume of 100 µl
	p53 of 20 µg or 50 mM MAPK siRNA incorporated into 44 mM Na_2CO_3, followed by 5 mM $CaCl_2$. DMEM-10% FBS was incorporated to achieve a final volume of 100 µl
CO_3AP	p53 of 20 µg or 50 mM MAPK siRNA was incorporated into 44 mM Na_2CO_3, followed by 5 mM $CaCl_2$; 1 µg of Tf was added before the incorporation of DMEM-10% FBS to obtain a final volume of 100 µl
	p53 of 20 µg or 50 mM MAPK siRNA was incorporated into 44 mM Na_2CO_3, followed by 5 mM $CaCl_2$; 1 µg of Fb was added before the incorporation of DMEM-10% FBS to obtain a final volume of 100 µl
Untreated	A volume of 100 µl of PBS

tumor growth was supervised every day by measuring the width and length of the tumor lump using a caliper, beginning from the treatment day (day 14), for two consecutive weeks. The weight of each mouse was observed daily for any significant changes. The mice were sacrificed by cervical dislocation at the study endpoint (day 28), followed by observation of organ morphology and potential metastasis of selected mice.

Results and discussion

Fabrication and characterization of LCSNPs

The generation of particles was accompanied by particle growth and aggregation, as reflected in the measured turbidity at the wavelength of 320 nm (Fig. 1a). Simple precipitation following a reaction between $SrCl_2$ and Na_2SO_3 resulted in the formation of large aggregates of $SrSO_3$ compared to SrF_2 particles, which formed after the reaction between

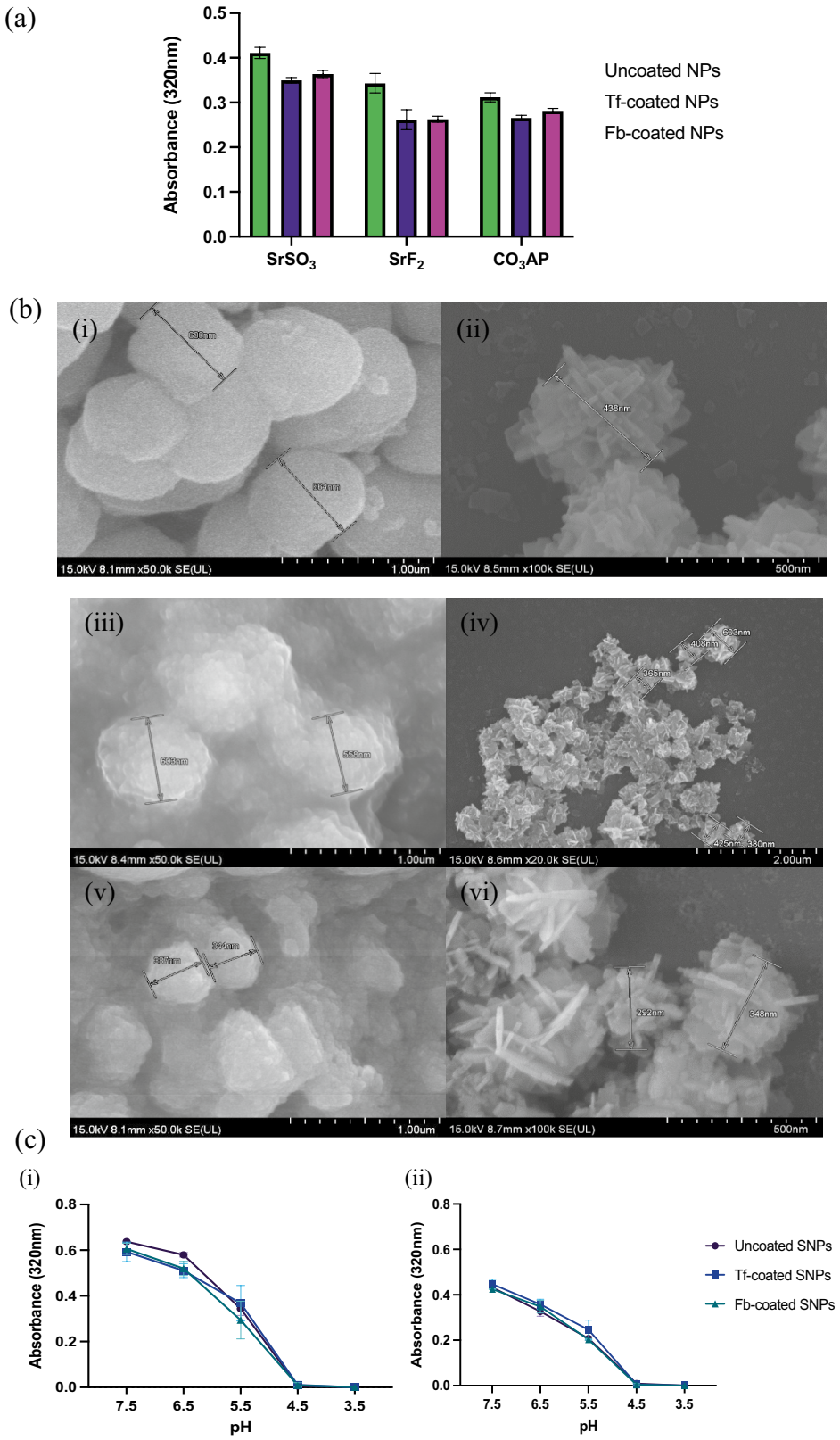

Fig. 1 Fabrication of LCSNPs. 5 µl of 1 M $SrCl_2$ was introduced into 5 µl HEPES buffered media (pH 7.5), followed by mixing of 2 µl of 1 M Na_2SO_3 or NaF, and incubated at 37 °C for 30 min. 1 µg of Tf or Fb was added to the suspension of the generated SNPs and further incubated for 10 min at 37 °C. **a** Absorbance following fabrication of LCSNPs was measured at 320 nm with reference to CO_3AP. **b** FE-SEM images of LCSNPs: (i) uncoated $SrSO_3$; (ii) uncoated SrF_2; (iii) Tf-complexed $SrSO_3$; (iv) Tf-complexed SrF_2; (v) Fb-complexed $SrSO_3$; (vi) Fb-complexed SrF_2. **c** Absorbance following introduction of HCl into fabricated SNPs was identified at 320 nm: (i) $SrSO_3$; (ii) SrF_2

Table 4 Particle size, zeta potential and PDI of LCSNPs

Salt formulation	Average size (nM)	Zeta potential (mV)	PDI
$SrSO_3$	354 ± 30	−2.20	0.315
Tf-$SrSO_3$	302 ± 41	−2.45	0.345
Fb-$SrSO_3$	275 ± 36	−2.55	0.305
SrF_2	119 ± 12	−2.93	0.256
Tf-SrF_2	95 ± 11	−3.31	0.217
Fb-SrF_2	73 ± 9	−3.48	0.193
CO_3 AP	257 ± 38	−2.04	0.290
Tf-CO_3 AP	247 ± 27	−2.89	0.346
Fb-CO_3 AP	176 ± 26	−2.74	0.278

$SrCl_2$ and Na_2SO_3, and CO_3 AP particles (positive control) fabricated according to the standard procedure (mentioned in the earlier studies).

Surface functionalization of SNPs, particularly SrF_2 with Tf and Fb showed less aggregation as reflected by the low turbidity. Investigation via ZetaSizer revealed the formation of smaller fabricated particles upon association with Fb and Tf (Table 4), with a reduction in average particle diameter ranging from 15 to 40%, in comparison to unmodified particles. FE-SEM imaging revealed an approximately 20–50% decline in size with Fb and Tf complexation. Essentially, the morphology of uncoated and coated $SrSO_3$ and SrF_2 remained identical, visualized as spherical and tiny rod-shaped particles, respectively (Fig. 1b).

The size of nanomaterials influences the extent of tumor accumulation. Smaller particles accumulate more rapidly and diffuse deeper into the tumor interstitium, allowing efficient transportation of genetic materials via passive targeting (Bertrand et al. 2014; Yetisgin et al. 2020). Huo et al. revealed that the 50 nm NPs penetrated more deeply into tumor spheroids than the larger NPs, which were primarily localized in the periphery of tumor spheroids (Huo et al. 2013). Size reduction is likely associated with electrostatic interactions between ligands and SNPs, which condenses the ionic constituents and stabilizes the particle structure (Hosseinkhani et al. 2013). The incorporation of cationic polymers including polyethyleneimine and poly(L-lysine) increases the surface charge of NPs, improving their interactions with negatively charged nucleic acids. Highly positively charged particles are, however, toxic to cells, which limits their in vivo application (Zhou and Pang 2018). The use of smaller-sized SNPs allows for more efficient particle deposition and localization through enhanced permeability and retention (EPR) effects. The design of an ideal carrier system is primarily guided by a few crucial factors, such as avoidance from macrophagic internalization, reduction in renal clearance, and evasion from microvascular occlusion (Patra et al. 2018). Structural morphology of spherical $SrSO_3$ confers greater surface areas to facilitate cellular attachment and internalization (Bakhtiar and Chowdhury 2021). Rod-shaped SrF_2 is thought to lessen the drag force of carrier structure to profoundly improve the internalization activity (Banerjee et al. 2016). Evident dissimilarity in size determined by FE-SEM and zeta size measurements may be attributed to the sputtering step in FE-SEM that caused large kinetic energy, which substantially increased the particle growth (Waykar et al. 2016).

An increase in zeta potential activity is likely to improve SNPs biodistribution. The risk of premature degradation in the circulatory system lowers as particle neutralizes, through protection from the binding of scavenging plasma proteins onto the surfaces, which would otherwise promote elimination through the mononuclear phagocyte system (Sathyamoorthy and Dhanaraju 2016). The presence of ligands creates more negatively charged SNPs that may consequently influence the interaction between anionic syndecan of the cellular membrane and negatively charged particles. However, functionalized NPs involving Tf and Fb proteins may improve cell adhesion and internalization activity via receptor-mediated endocytosis (Pandit et al. 2020).

The homogenous size distribution as determined by polydispersity index (PDI) is a vital characteristic for an efficient and safe nucleic acid transporter. An appropriate PDI is a prerequisite to determining the accumulation activity at the target organ or tissue that is highly dependent on size distribution. A value of 0.3 or lower is most desirable as it indicates a relatively homogeneous size distribution of NPs. Extremely monodisperse particle distribution is identified by a PDI value of < 0.05, while the values of > 0.7 indicate polydispersity (Danaei et al. 2018). SrF_2 was considered monodispersed with the PDI values read between 0.193 and 0.256 as compared to readings between 0.305 and 0.345 measured in $SrSO_3$ (Table 4). Banerjee et al. revealed that a PDI value of < 0.2 is most favorable but further explained that size distribution might be difficult to maintain, especially in the biological system as constituents of NPs may interact with biological components within the blood, which can modify the degree of dispersity (Banerjee et al. 2016). Changes from small to large-scale particle production, especially in clinical experimentations, may further influence the particle distribution; therefore, continuous monitoring should be performed extensively (Patra et al. 2018).

Investigation on pH-responsive characteristic of LCSNPs was performed through introduction of acidic pH to mimic the late endosomal stage. The later endosome has pH of

approximately 3.5–4.5, where SNPs was able to disintegrate and to release pDNA via proton sponge effect (Bakhtiar and Chowdhury 2021). Dissolution of the particles within endosomal cavity should lead to accumulation of cations and anions, causing high osmoticity within the cavity, resulting in the swelling and rupturing the SNPs. Spectrophotometric reading revealed effective dissolution of $SrSO_3$ and SrF, as absolute particles dissolution occurs at pH 4.5, seen by 0.0 in absorbance intensity (Fig. 1c). Incorporation of ligands on both SNPs revealed similarly efficient responses in dissolution activity that is vital to prevent inefficient escape of genetic materials that may impede transfection activity, resulting in lower transgene expression or inefficient silencing of an endogenous gene (Hossain et al. 2010). It is expected that the salt particles would be able to maintain their structures especially in the blood which is slightly basic, with pH range of about 7.35–7.45. With the pH ranging from 7.0 to 7.4 in average physiological tissues, SNPs will not disintegrate prematurely to release their genetic load, thus promoting the gene activity (expression or silencing) particularly in the targeted cancer cells (Huang and Guo 2011; Morachis et al. 2012).

Loading efficiency and cellular uptake analysis of LCSNPs

Investigation on cellular uptake is an important step to determine the transcellular fate of the nucleic acid-loaded carrier. Fluorescence microscopic observation with fluorescent pGFP and AF 488-tagged SNPs treatment unveiled the presence of genetic materials that are either associated with the plasma membrane or endocytosed complexes (Fig. 2).

Notably, the fluorescence signal was evident with different nucleic acid treatments, which may be associated with effective cellular uptake to mitigate cell-mediated endocytosis. There are several ways known by which NPs can enter the cells, which include energy-dependent and non-energy-dependent pathways. Large ionic molecules cannot easily cross the phospholipid bilayers of the cell membrane, thus an energy-dependent endocytosis process is acquired for internalization (Yang and Hinner 2015). Upon ligand conjugation, negatively charged particle surface was not implicated undesirably in terms of interaction with the cellular surface as reflected by the significantly stronger signal from LCSNPs-treated groups. Niikura et al. reported the better uptake of the rod-like NPs based on particle quantity while spherical particles were found more grounded based on the weight of NPs (Niikura et al. 2013). In terms of gene delivery, one of the attractive features of functionalized nanocarriers is that the positively charged strontium ion domains of SNPs interact effectively with the cellular membrane, in addition to the presence of an active mechanism involving ligands interacting with the overexpressed receptors on the carcinoma cellular surface, which allows for effective transcytosis (Guerrini et al. 2018; Pesce et al. 2013). A study by Zhang et al. further suggested that the most ideal uptake of ligand-mediated NPs occurred with the introduction of particle size of 50 nm in diameter (Zhang et al. 2009).

In vitro gene transfection with LCSNPs

Efficient transgene expression or knockdown of an endogenous gene necessitates the transport of plasmid DNA and siRNA with the help of SNPs to either nucleus or cytosol, respectively. The use of reporter plasmids including green fluorescent protein (pGFP) and firefly luciferase (pGL3) allows for a distinctly sensitive and powerful approach in determining the effectiveness of the potential carrier to facilitate the gene transfer and expression in the nucleus, as determined by the presence of fluorescent and luminescent signals (Pajarinen et al. 2015). The intracellular carrier potentiality is determined by nucleic acid escape from the particle complexes before the content is subjected to the lysosomal degradation or exocytosis via a transcellular pump located in the cellular membrane (Saric and Freeman 2021).

The high fluorescence-expressing cells suggest an effective gene release from LCSNPs in contrast to uncoated groups (Fig. 3). The expression of pGL3 on MCF-7 reportedly resulted in more than 10X greater luminescence of SrF_2 conjugated with Tf and Fb than that of non-functionalized groups (Fig. 3b); the signal was also more significant than that of $SrSO_3$ and CO_3 AP. In contrast, 4T1 bioluminescence activity identified with ligand-$SrSO_3$ complexes revealed maximum emission of approximately 10X more RLU/mg protein in comparison to SrF_2 and CO_3 AP. This, in turn, shows a significant improvement in transgene activity of reporter genes transported by LCSNPs that combines the efficient cellular uptake and DNA escape via pH-dependent strontium salt disintegration based on the "proton-sponge" hypothesis (Bakhtiar and Chowdhury 2021).

Loss of function in p53, a prominent tumor suppressor, often correlates with cancer onset and progression besides treatment resistance. Delivery of the wild-type p53 to tumor cells is believed to restore the normality in the regulatory mechanism of the "guardian of the genome" that is often absent or malfunctioned (Kotcherlakota et al. 2019). Unloaded SNPs were shown to result in 95% viability as compared to untreated groups (reflected as 100%), suggesting reasonable safety in vitro. MCF-7 and 4T1 cells treated with SNPs-loaded p53 plasmid DNA reacted greatly upon Fb coating, as demonstrated by cell death of as high as 70% (Fig. 4).

Results show that the introduction of the Tf-conjugated SNPs resulted in apparent cellular apoptosis as compared to uncoated SNPs, although less than that of Fb-coated groups,

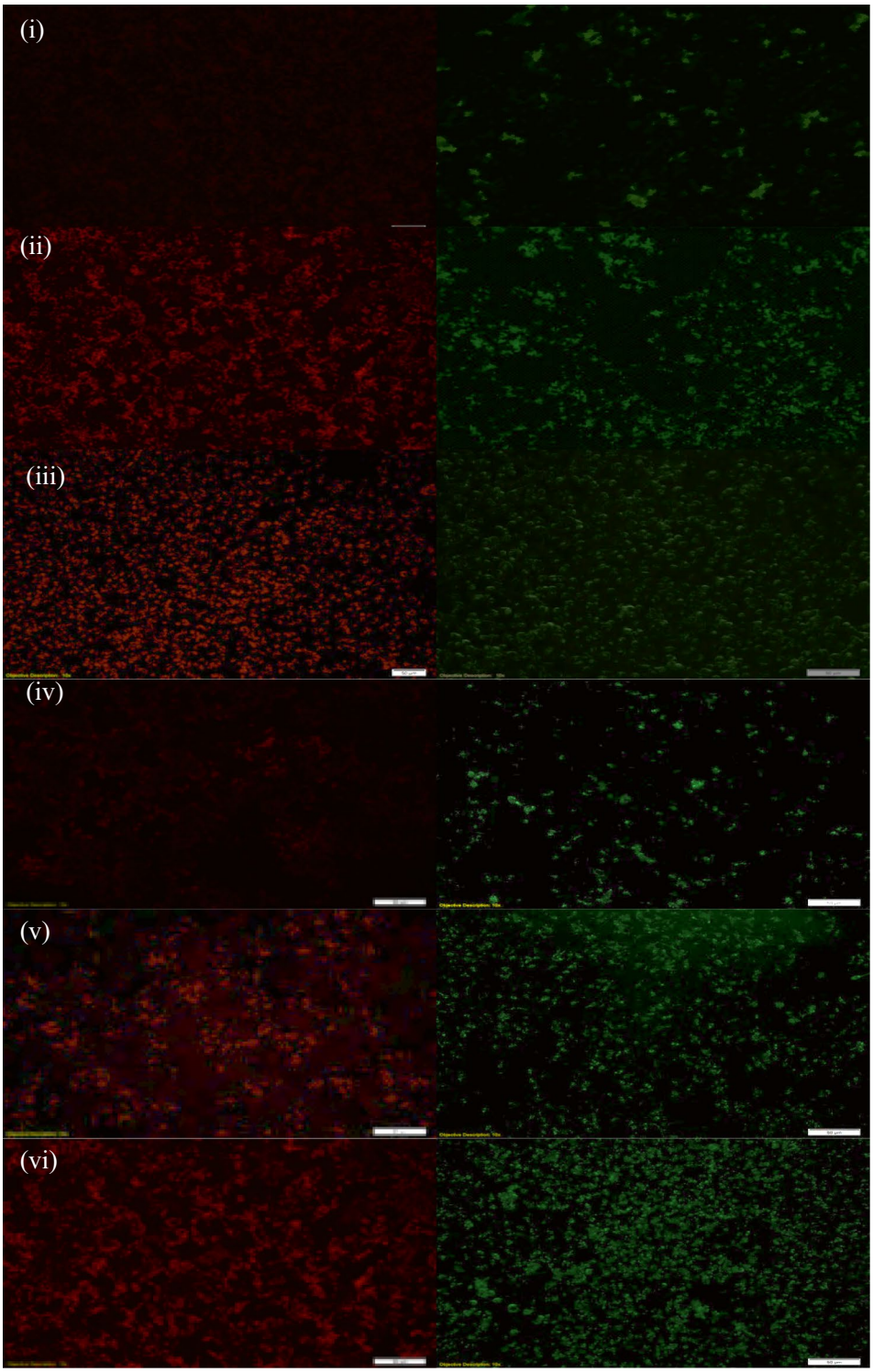

Fig. 2 MCF-7 cells uptake of PI-labeled GFP-loaded LCSNPs (left) and AF-488-loaded LCSNPs (right). Transfected cells were incubated for 4 h, prior to washing with EDTA in 1X PBS and addition of 100 µl DMEM. Fluorescence images of (i) uncoated $SrSO_3$; (ii) Fb-coated $SrSO_3$; (iii) Tf-coated $SrSO_3$; (iv) uncoated SrF_2; (v) Fb-coated SrF_2; (vi) Tf-coated SrF_2 captured at 10X resolution (Scale bars = 50 µm)

indicating the association of p53 expression with induced apoptosis in both mammary carcinoma cells. MCF-7 viability was significantly low at 72 h, as exhibited by Fb-coated p53-loaded SrF_2 and Fb-coated p53-loaded $SrSO_3$ with 30% and 45% viable cells, respectively. Similarly, the cell viability of 4T1 was approximately 27% and 36% after treatments with Fb-coated p53-loaded SrF_2 and Fb-coated p53-loaded $SrSO_3$, respectively. CO_3 AP functionalized with Fb and Tf only showed superior apoptotic activity against 4T1 cells, which was significantly less than SNP complexes. The morphology of LCSNPs is a clear parameter that directly affects the intracellular trafficking of nanoparticles. Studies have found that

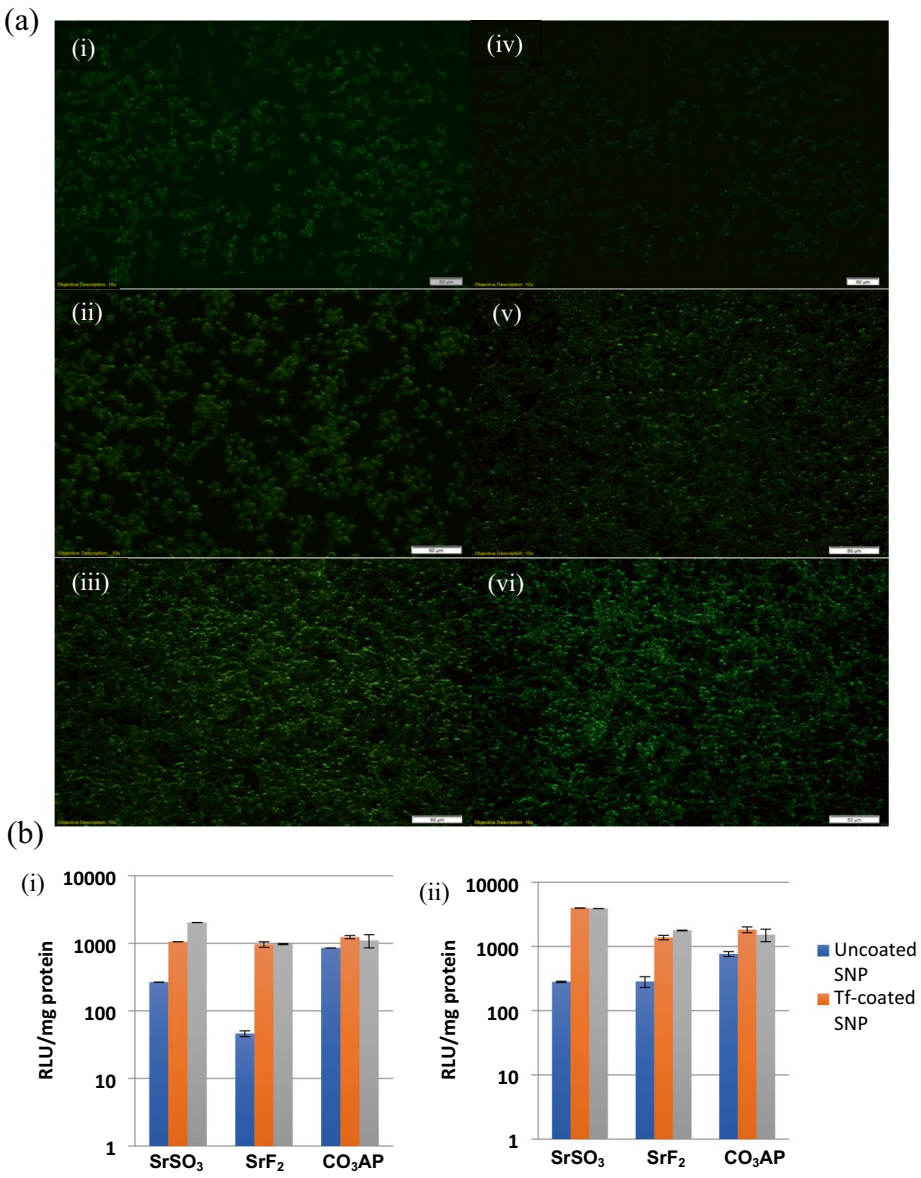

Fig. 3 In vitro gene transfection activity of LCSNPs. **a** Fluorescence positive cells owing to expression of pGFP after intracellular delivery with SNPs in MCF-7 cells. Transfected cells were incubated for 4 h, prior to washing with EDTA in 1X PBS and additional 48 h incubation. (i) $SrSO_3$; (ii) Tf-$SrSO_3$; (iii) Fb-$SrSO_3$; (iv) SrF_2; (v) Tf-SrF_2; (vi) Fb-SrF_2 were observed under FITC-filtered fluorescence microscope. **b** Luminescence intensity of LCSNPs-treated (i) MCF-7 and (ii) 4T1 cells. Transfected cells were incubated for 48 h after substitution of serum-supplemented media following first 4 h of incubation. Cells were lysed following removal of media, and the remaining lysate was centrifuged to obtain the supernatant to measure the relative luminescence activity (RLU) in treated cells. (Scale bars = 50 µm)

rod-like NPs have higher internalization rates than the spheres, cylinders, and cubes, as demonstrated by better surface area and surface adherence ability for protein conjugation, enabling effective receptor targeting to facilitate cellular transcytosis (Foroozandeh and Aziz 2018; Behzadi et al. 2017). The spherical structure of $SrSO_3$ also ensures good surface area for ligand-induced internalization (Li et al. 2015), as seen by the reduction in cell viability.

Analysis of MAPK and AKT pathway following intracellular delivery of MAPK siRNA

MAPK/ERK pathway plays vital roles in the proliferation and survival of cancer cells, apart from the ability to crosstalk with one another via activation of key proteins including MAPK and Akt. The introduction of MAPK siRNA is thought to block the downstream pathway via inhibition of p44/42 MAP kinase expression and silencing of ERK1/2 genes (Lu et al. 2019). To determine the silencing activity in LCSNPs-treated cells, Western blot analysis was performed.

The present study revealed a remarkable decrease in both total and phosphorylated MAPK and AKT levels in Fb-conjugated SNPs treated groups, suggesting superior knockdown activity on MCF-7 cells (Fig. 5). Treatment with Tf-coated SNPs resulted in weakened band intensity of total and phosphorylated MAPK as compared to uncoated groups. Successful siRNA-mediated knockdown of MAPK/ERK signaling further proves the relationship in ligand-receptor attachments and improved the cellular

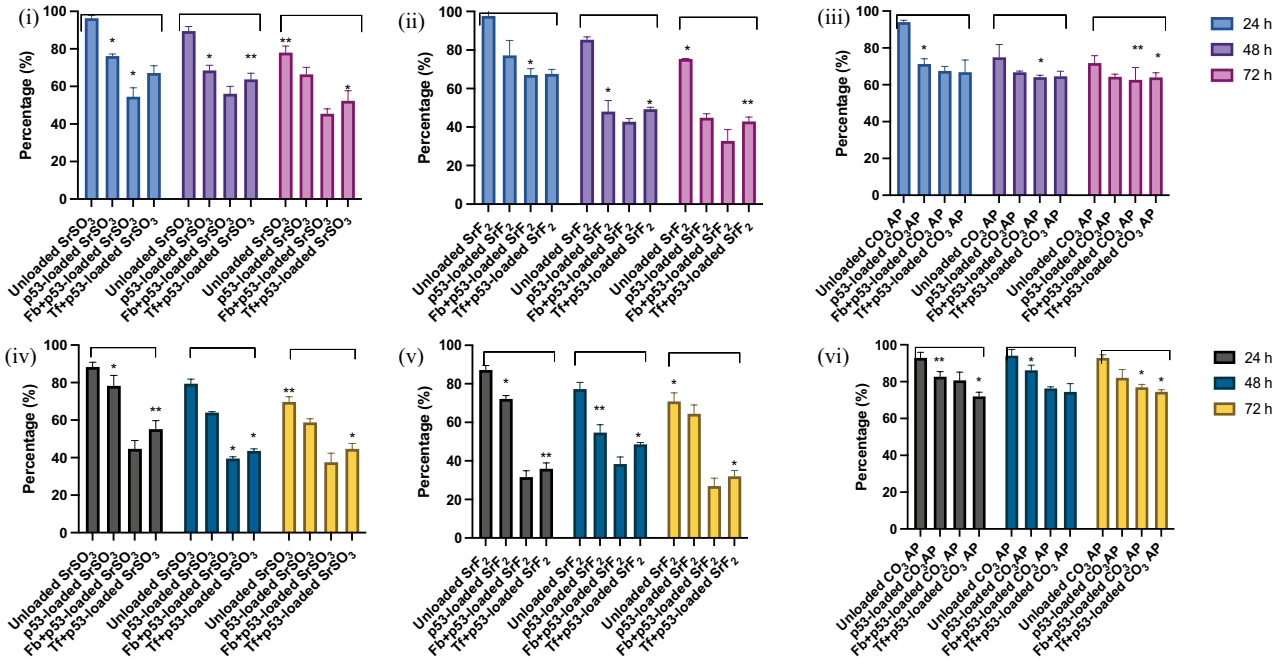

Fig. 4 Cell viability (%) following treatment of LCSNPs loaded with p53 plasmid. Seeded cells were treated with p53-loaded SNP with respective 1 µg Tf-/Fb-coated SNPs. MTT assay was performed on the MCF-7 cells treated with (i) $SrSO_3$, (ii) SrF_2 and (iii) CO_3 AP and 4T1 cells treated with (iv) $SrSO_3$, (v) SrF_2 and (vi) CO_3 AP. 50 µl of MTT solution was incorporated into the treated cells and MTT containing media was removed after 4 h, followed by introduction of 300 µl of DMSO. Spectrophotometric reading was taken at 570 nm wavelength, reference to 630 nm. Cell viability of each sample group was presented as mean ± SD (%). The asterisks *, ** represented significant difference at $p < 0.05$ and $p < 0.01$, respectively

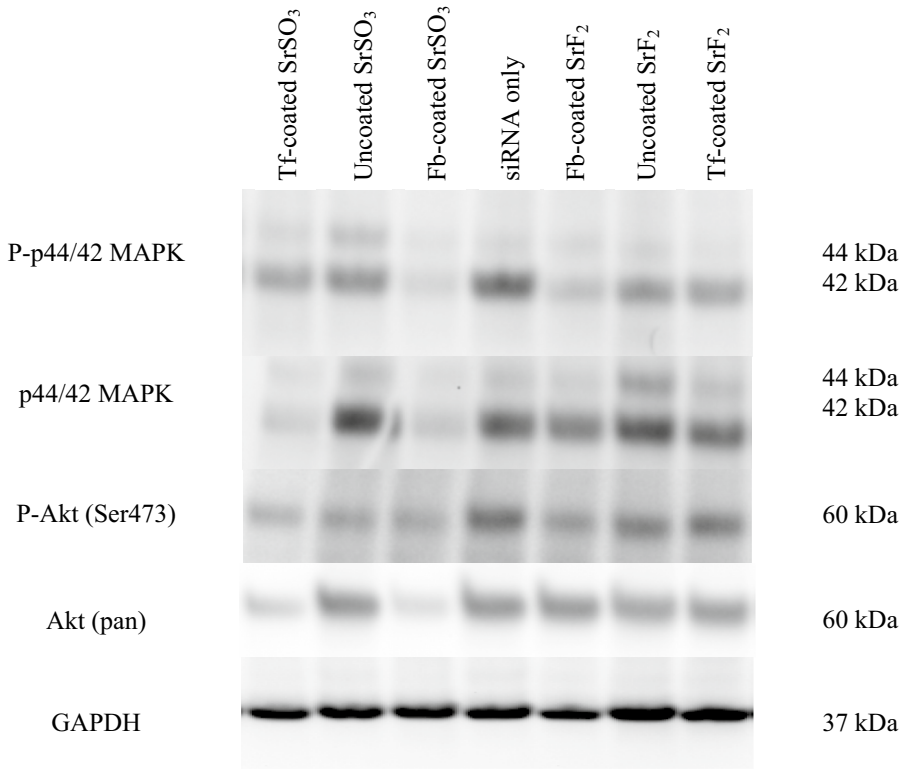

Fig. 5 Protein expression following treatment of MCF-7 cells with LCSNPs loaded with MAPK siRNA. Proteins obtained from lysates of treated cells were run on SDS-PAGE and transferred to PVDF membrane, followed by incubation with primary antibodies raised in rabbit against phosphor-p44/42 MAPK, p44,42 MAPK, phosphor-Akt (Ser473) and Akt (pan). HRP-conjugated goat anti-rabbit secondary antibody was used to detect the chemiluminescence signals. Predicted bands for pMAPK, TMAPK, pAkt and Takt are at 44, 42 and 60 kDa, respectively. GAPDH was used as loading marker with bands achieved at 37 kDa

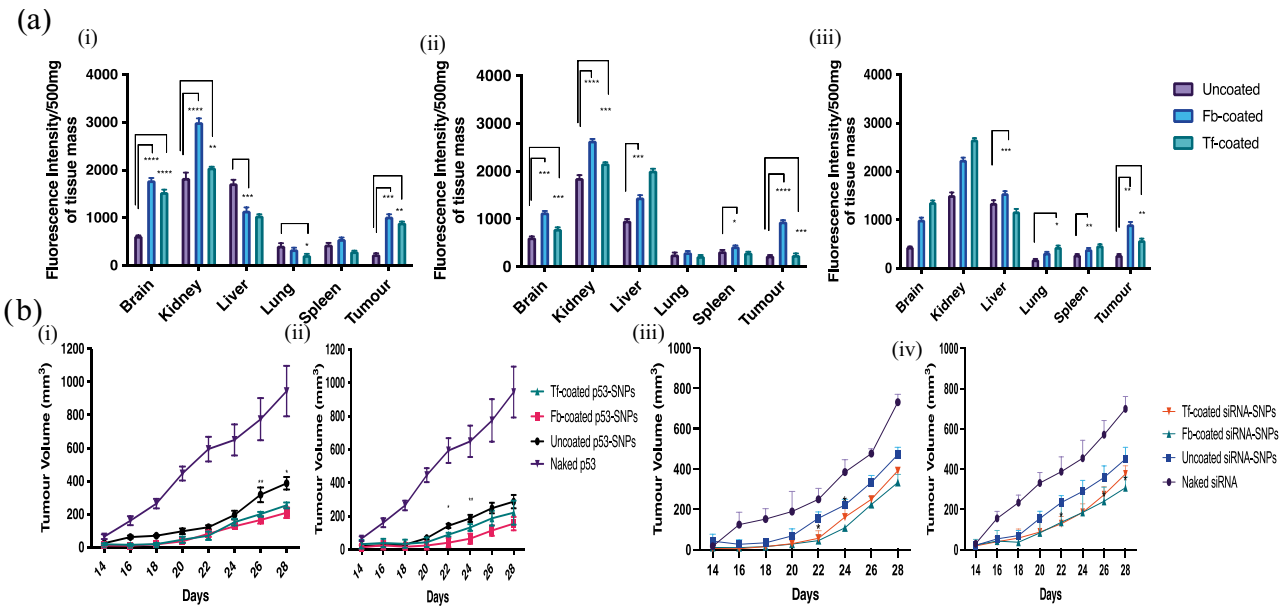

Fig. 6 In vivo gene activity on tumor xenograft mice models. **a** Biodistribution following intravenous delivery of LCSNPs loaded with AF 488 siRNA was performed following (i) $SrSO_3$, (ii) SrF_2 and (iii) CO_3 AP intravenous injection. Mice were sacrificed 4 h post treatment, followed by organs harvesting and lysis. Tissue lysates were centrifuged at 15,000 RPM for 30 min at 4 °C; 100 µl supernatant was aspirated to detect fluorescence activity of each organ. **b** Tumor regression activity following intravenous delivery of LCSNPs loaded with p53 plasmid and MAPK siRNA. 4T1-tumor induced mice were treated intravenously with 100 µl suspension of SNPs fabricated by 5 µl 1 M $SrCl_2$ and 2 µl 1 M Na_2SO_3/NaF with 20 µg p53 or 50 nM MAPK siRNA in 10 µl HEPES, and complexed with 1 µg Fb or Tf, as the tumor volume reached approximately 100 mm^3. Naked p53 and uncoated SNPs represented negative control. Second dose was administered 2 days following the first treatment (− day 17). Tumor growth was monitored every two days, continuously for two weeks. plasmid-loaded (i) $SrSO_3$, (ii) SrF_2 and siRNA loaded (iii) $SrSO_3$, (iv) SrF_2. $^{**}p < 0.01$ and $^{*}p < 0.05$ as compared to uncoated SNP

uptake and pH-dependent dissolution of the endocytosed particles to unravel the siRNA cargo into the cytosol (Butti et al. 2018).

Tissue biodistribution of LCSNPs

Biodistribution activity of ligand-coated SNPs labeled with fluorescence siRNA was investigated following intravenous administration into the tumor-bearing mice (Fig. 6a). The injections were well-tolerated, and mice did not exhibit any behavioral changes. The mice were sacrificed, dissected and the organs were harvested for fluorescence intensity measurement. The untreated group was used for the normalization of the data.

Different levels of fluorescence intensity were detected in the liver, kidney, brain, lung, spleen, and tumor at 1 h post-intravenous delivery where the kidneys remained the preferential sites for all study groups. Overcoming the RES has been a crucial obstacle in the application of nanoparticles as a gene carrier. The RES is part of the immune response system that engulfs NPs and transports them into reticuloendothelial organs, present primarily in the liver (Kupffer cells), kidneys (intraglomerular mesangial cells), spleen, and lungs. Nanoparticle retention in RES organs results in inefficient tumor targeting and penetration, in addition to the long-term concerns regarding the toxicity of NPs, especially those comprising toxic elements (Tang et al. 2019). The introduction of Fb- and Tf-coated SNPs revealed lower deposition in the liver cells while being more localized in the brain and tumor cells as compared to uncoated groups. AF 488-loaded SNPs conjugated with Fb resulted in up to three-fold increment in trans-tumoral accumulation. Tf was associated with lower tumor localization than that of Fb-coated complexes, but significantly higher than that of uncoated groups. Notably, treatment with Fb-coated CO_3AP also resulted in high siRNA accumulation in tumor and brain tissues.

High tumor accumulation of Fb-coated nanocarriers may be attributed to the presence of overly expressed Integrin α5β1, the Fb receptor that modulates numerous signaling pathways that are associated with aggressiveness in carcinoma cells, particularly in breast, colon, ovarian, lung, and brain (Schaffner et al. 2013). Tf receptor, an iron importer, is overexpressed in many malignant cells (up to a 100-fold increase) due to the high demand for iron that is essential for tumorigenesis and carcinoma growth (Shen et al. 2018). Tortorella and Karagiannis reported that upregulation in the expression of

the transferrin receptor in many solid cancers and brain glioma resulted in the successful delivery of anticancer agents to the tumor site, which is attributed to the ability to penetrate the blood brain barrier (BBB) (Tortorella and Karagiannis 2014), as similarly demonstrated in this study. Delivery of pharmacotherapy to the brain is hindered by the BBB except for small hydrophilic materials of < 150 Da or highly hydrophobic components of < 600 Da, limiting the effectiveness of both conventional and novel therapies at the targeted site. Kong et al. found that multifunctional NPs modified with arginine-glycine-aspartic peptide resulted in significantly high gene knockdown up to 50.8%. It was proposed that the binding to αvβ3 integrin receptor allows NPs to overcome the complexity of physiological features of BBB (Kong et al. 2017).

It is suggested that the transportation of $SrSO_3$ and SrF_2 into the tumor tissues was contributed by both active and passive targeting mechanisms, which significantly improved the accumulation in cancer tissues. Particle size affects the accessibility of target organs, the mode of cellular uptake, and the efficiency of the endocytic pathway, which are the important parameters for an ideal gene vector (Liu and Auguste 2015). The diameter of NPs also influences the mode of excretion as the particles with a hydrodynamic diameter of < 10 nm are often eliminated via renal elimination while larger particles are excreted through the liver (Danaei et al. 2018). Nonetheless, it is evident that smaller-sized SNPs are not only sufficient for therapeutic efficacy, but the roles of ligand-mediated internalization also play a vital role in the outcome of the nanocarrier system (Bertrand et al. 2014; Clemons et al. 2018).

Tumor regression activity of LCSNPs

Naked pDNA and siRNA are readily degraded by endogenous enzymes and cleared by kidneys, resulting in short half-life and low nucleic acid accumulation in tumor tissues. Opsonin proteins adhere to foreign objects to allow visibility to the mononuclear phagocytic system (MPS), resulting in the clearance of uncoated NPs from the circulatory system [47]. Without a vector, pDNA and siRNA will be removed from the circulatory system within 5 and 15 min, respectively, following systemic administration (Gao et al. 2009; Walther et al. 2006).

In the previous study, we demonstrated significant cellular growth retardation in 4T1 tumor-induced xenograft models inoculated with p53 plasmid DNA and p44/42 MAPK siRNA loaded into both $SrSO_3$ and SrF_2 based on the tumor growth as compared to controls. Intravenous delivery of p53 pDNA and MAPK siRNA-loaded SNPs complexes were well-tolerated, whereby all animals survived and were euthanized after four weeks of experimentation. Two doses of intravenous administration of Tf- and Fb-coated SNPs resulted in a reduction of tumor volume as compared to that of control groups (naked p53 and uncoated SNPs) (Fig. 6b). Interestingly, there were no tumor-free animals observed, and both Tf- and Fb-coated SNPs groups significantly decelerated the tumor growth by approximately two to threefold in comparison to naked genetic delivery. The analysis further showed that the introduction of Fb-conjugated SNPs led to approximately 50% inhibition in tumor growth, based on the size, as compared to that of uncoated groups as measured on day 14. The tumor growth rate in the Fb-coated SNPs-treated groups was lower than that of Tf-coated SNPs-treated groups, as evident by approximately 50 mm^3 of tumor volume difference on day 28. Tf-functionalized SNPs resulted in a slightly large tumor volume. Fb-coated SrF_2 significantly slowed the tumor growth as compared to Fb-coated $SrSO_3$, with > 50 mm^3 tumor volume difference observed on day 28. There was no sign of metastasis in both lungs and liver, and the overall treatment resulted in no changes in the survival rate of all treated groups. The introduction of Tf and Fb into SNPs loaded with MAPK siRNA also led to a reduction in overall tumor volume (Fig. 6b). Tumor size was the smallest with treatment using Fb-coated SNPs, with a size approximately 100 and 380 mm^3 smaller than Tf-SNPs and uncoated SNPs groups, respectively.

Nanomaterials engineered with Tf and Fb anchored to SNPs confer effective tumor tissue localization and retention through the EPR effect and facilitate gene transport across the plasma membrane via receptor-mediated active transport mechanism. Upon endocytosis, encapsulated particle complex undergoes degradation following the gradual drop in pH due to absorption of intracellular protons at the late endosomal phase, destabilizing the endosomal membrane and sequentially releasing the genetic content to the cytosol (Foroozandeh and Aziz 2018; Almeida et al. 2021). Both p53 pDNA and siRNA require protection against numerous extracellular and intracellular barriers, which severely compromise their availability in the cytosol. However, unlike pDNA which requires transcriptional machinery in the nucleus, siRNA does not require an entry into the nucleus as it cleaves the target mRNA in the cytosol. The tumor growth rate of LCSNPs was notably slower than that of non-functionalized groups, indicating greater nucleic acid activity against murine mammary carcinoma cells through modification in particle size and tissue targeting activity (Gao et al. 2021; Kim et al. 2015).

Conclusion

We investigated the potential ability of ligand coating in improving the activity of pH-responsive $SrSO_3$ and SrF_2 NPs to transport the pDNA and siRNA both in vitro and in vivo. Incorporation of both Tf and Fb is deduced to have expanded the potential activity of $SrSO_3$ and SrF_2 as biological carriers of genetic materials by tuning the size of fabricated particles and promoting receptor-mediated cellular internalization to eventually release the therapeutic cargo into the target cells. Fb- and Tf-bound SrF_2 and $SrSO_3$ demonstrated significant cytotoxicity against both MCF-7 and 4T1 cells in comparison to control groups, proving the impact of active targeting on the intracellular trafficking and the final therapeutic efficacy of nucleic acids-loaded SNPs. The biodistribution profiles of Tf- and Fb-coated SNPs suggest major accumulation of the SNPs in the RES organs, similar to uncoated SNPs. However, tumor tissue deposition was immensely higher with Tf- and Fb-coated SNPs than the uncoated SNPs, suggesting that receptor-mediated endocytosis might lead to subsequent effective internalization of the NPs. Enhanced tumor growth inhibition observed in LCSNPs directly correlates to the tumor accumulation of transported genetic cargo. Surface functionalization of the SNPs with hydrophilic macromolecules, such as polyethylene glycol might reduce the particle surface charge with concomitant improvement in tumor targeting and consequential anti-tumor activity. Further study on the long-term effects of surface-modified SNPs is required to evaluate their potential implications in clinal gene therapy.

Acknowledgements The authors acknowledge the financial support received from the Ministry of Science, Technology & Innovation, Malaysia (Project ID: 02-02-10-SF0083) and SEED Grant, School of Pharmacy, Monash University Malaysia.

Funding Open Access funding enabled and organized by CAUL and its Member Institutions. Kementerian Sains, Teknologi dan Inovasi,02–02-10-SF0083, Ezharul Hoque Chowdhury, Monash University Malaysia, SEED-01/2020, Athirah Bakhtiar

Declarations

Conflict of interest All authors (A. Bakhtiar, Q.X. Liew, K.Y. Ng, and E.H. Chowdhury) declare that they have no conflict of interest.

Ethical approval The animal studies were performed after receiving approval of Monash University Animal Ethics Committee: MARP/2012/087. All applicable international, national, and/or institutional guidelines for the care and use of animals were followed.

References

Almeida MS, Susnik E, Drasler B, Taladriz-Blanco P, Petri-Fink A et al (2021) Understanding nanoparticle endocytosis to improve targeting strategies in nanomedicine. Chem Soc Rev 50:5397–5434

Bakhtiar A, Chowdhury EH (2021) pH-responsive strontium nanoparticles for targeted gene therapy against mammary carcinoma cells. Asian J Pharm Sci 16(2):236–252

Bakhtiar A, Aik Seng N, Khuen Yen N, Chowdhury EH (2021) In vivo evaluation of biodistribution and toxicity of pH-responsive strontium nanoparticles for gene delivery. J Pharm Investig. https://doi.org/10.1007/s40005-021-00547-7

Banerjee A, Qi J, Gogoi R, Wong J, Mitragotri S (2016) Role of nanoparticle size, shape and surface chemistry in oral drug delivery. J Control Release 238:176–185

Bazak R, Houri M, El Achy S, Kamel S, Refaat T (2015) Cancer active targeting by nanoparticles: a comprehensive review of literature. J Cancer Res Clin Oncol 141(5):769–784

Behzadi S, Serpooshan V, Tao W, Hamaly MA, Alkawareek MY et al (2017) Cellular uptake of nanoparticles: journey inside the cell. Chem Soc Rev 46(14):4218–4244

Bertrand N, Wu J, Xu X, Kamaly N, Farokhzad OC (2014) Cancer nanotechnology: the impact of passive and active targeting in the era of modern cancer biology. Adv Drug Deliv Rev 66:2–25

Butti R, Das S, Gunasekaran VP, Yadav AS, Kumar D et al (2018) Receptor tyrosine kinases (RTKs) in breast cancer: signaling, therapeutic implications and challenges. Mol Cancer 17:34

Candelaria PV, Leoh LS, Penichet ML, Daniels-Wells TR (2021) Antibodies targeting the transferrin receptor 1 (TfR1) as direct anticancer agents. Front Immunol 12:607692

Chen J, Guo Z, Tian H, Chen X (2016) Production and clinical development of nanoparticles for gene delivery. Mol Ther Methods Clin Dev 3:16023

Clemons TD, Singh R, Sorolla A, Chaudhari N, Hubbard A et al (2018) Distinction between active and passive targeting of nanoparticles dictate their overall therapeutic efficacy. Langmuir 34(50):15343–15349

Danaei M, Dehghankhold M, Ataei S, Davarani FH, Javanmard R et al (2018) Impact of particle size and polydispersity index on the clinical applications of lipidic nanocarrier systems. Pharmaceutics 10(2):57

Daniels TR, Bernabeu E, Rodríguez JA, Patel S, Kozman M et al (2012) The transferrin receptor and the targeted delivery of therapeutic agents against cancer. Biochim Biophys Acta 1820(3):291–317

Deshpande PP, Biswas S, Torchilin VP (2013) Current trends in the use of liposomes for tumor targeting. Nanomedicine 8(9):1509–1528

Durymanov M, Reineke J (2018) Non-viral delivery of nucleic acids: insight into mechanisms of overcoming intracellular barriers. Front Pharmacol 9:971

Foroozandeh P, Aziz AA (2018) Insight into cellular uptake and intracellular trafficking of nanoparticles. Nanoscale Res Lett 13:339

Gao S, Dagnaes-Hansen F, Nielsen EJ, Wengel J, Besenbacher F et al (2009) The effect of chemical modification and nanoparticle formulation on stability and biodistribution of siRNA in mice. Mol Ther 17(7):1225–1233

Gao Y, Men K, Pan C, Li J, Wu J et al (2021) Functionalized DMP-039 hybrid nanoparticle as a novel mrna vector for efficient cancer suicide gene therapy. Int J Nanomedicine 16:5211–5232

Guerrini L, Alvarez-Puebla RA, Pazos-Perez N (2018) Surface modifications of nanoparticles for stability in biological fluids. Materials 11:1154

Hoshyar N, Gray S, Han H, Bao G (2016) The effect of nanoparticle size on in vivo pharmacokinetics and cellular interaction. Nanomedicine 11(6):673–692

Hossain S, Tada S, Akaike T, Chowdhury EH (2010) Influences of electrolytes and glucose on formulation of carbonate apatite nanocrystals for efficient gene delivery to mammalian cells. Anal Biochem 397:156–161

Hosseinkhani H, He WJ, Chiang CH, Hong PD, Yu DS et al (2013) Biodegradable nanoparticles for gene therapy technology. J Nanopart Res 15:1794

Huang L, Guo S (2011) Nanoparticles escaping RES and endosome: challenges for siRNA delivery for cancer therapy. J Nanomater 2011:12

Huo S, Ma H, Huang K, Lui J, Wei T et al (2013) Superior penetration and retention behavior of 50 nm gold nanoparticles in tumors. Cancer Res 73(1):319–330

Kim J, Wilson DR, Zamboni CG, Green JJ (2015) Targeted polymeric nanoparticles for cancer gene therapy. J Drug Target 23(7–8):627–641

Kong L, Qiu J, Sun W, Yang J, Shen M et al (2017) Multifunctional PEI-entrapped gold nanoparticles enable efficient delivery of therapeutic siRNA into glioblastoma cells. Biomater Sci R Soc Chem 5(2):258–266

Kotcherlakota R, Vydiam K, Srinivasan DJ, Mukherjee S, Roy A et al (2019) Restoration of p53 function in ovarian cancer mediated by gold nanoparticle-based EGFR targeted gene delivery system. ACS Biomater Sci Eng 5(7):3631–3644

Li Y, Kroger M, Liu WK (2015) Shape effect in cellular uptake of PEGylated nanoparticles: comparison between sphere, rod, cube and disk. Nanoscale 7:16631–16646

Lin TC, Yang CH, Cheng LH, Chang WT, Lin YR, Cheng HC (2019) Fibronectin in cancer: friend or foe. Cells 9(1):27

Liu D, Auguste DT (2015) Cancer targeted therapeutics: from molecules to drug delivery vehicles. J Control Release 219:632–643

Lu M, Wang Y, Zhan X (2019) The MAPK pathway-based drug therapeutic targets in pituitary adenomas. Front Endocrinol 10:330

Montaño-Samaniego M, Bravo-Estupiñan DM, Méndez-Guerrero O, Alarcón-Hernández E, Ibáñez-Hernández M (2020) Strategies for targeting gene therapy in cancer cells with tumor-specific promoters. Front Oncol 10:605380

Morachis JM, Mahmoud E, Sankaranarayanan J, Almutairi A (2012) Triggered rapid degradation of nanoparticles for gene delivery. J Drug Deliv 2012:1–7

Niikura K, Matsunaga T, Suzuki T, Kobayashi S, Yamaguchi H et al (2013) Gold nanoparticles as a vaccine platform: influence of size and shape on immunological responses in vitro and in vivo. ACS Nano 7:3926–3938

Pajarinen J, Lin TH, Sato T, Loi F, Yao Z et al (2015) Establishment of green fluorescent protein and firefly luciferase expressing mouse primary macrophages for in vivo bioluminescence imaging. PLoS ONE 10(11):e0142736

Pandit S, Dutta D, Nie S (2020) Active transcytosis and new opportunities for cancer nanomedicine. Nat Mater 19:478–480

Patra JK, Das G, Fraceto LF, Campos EVR, Rodriguez-Torres MdP et al (2018) Nano based drug delivery systems: recent developments and future prospects. J Nanobiotechnol 16:71

Pesce D, Wu Y, Kolbe A, Weil T, Herrmann A (2013) Enhancing cellular uptake of GFP via unfolded supercharged protein tags. Biomaterials 34(17):4360–4367

Ramamoorth M, Narvekar A (2015) Non viral vectors in gene therapy-an overview. J Clin Diagn Res 9(1):GE01-GE6

Rosenblum D, Joshi N, Tao W, Karp JM, Peer D (2018) Progress and challenges towards targeted delivery of cancer therapeutics. Nat Commun 9:1410

Sampayo RG, Toscani AM, Rubashkin MG, Thi K, Masullo LA et al (2018) Fibronectin rescues estrogen receptor α from lysosomal degradation in breast cancer cells. J Cell Biol 217(8):2777–2798

Saric A, Freeman SA (2021) Endomembrane tension and trafficking. Front Cell Dev Biol 8:611326

Sathyamoorthy N, Dhanaraju MD (2016) Shielding therapeutic drug carriers from the mononuclear phagocyte system: a review. Crit Rev Ther Drug Carrier Syst 33(6):489–567

Schaffner F, Ray AM, Dontenwill M (2013) Integrin α5β1, the fibronectin receptor, as a pertinent therapeutic target in solid tumors. Cancers 5(1):27–47

Shen Y, Li X, Dong D, Zhang B, Xue Y, Shang P (2018) Transferrin receptor 1 in cancer: a new sight for cancer therapy. Am J Cancer Res 8(6):916–931

Tang Y, Wang X, Li J, Nie Y, Liao G et al (2019) Overcoming the reticuloendothelial system barrier to drug delivery with a "Don't-Eat-Us" strategy. ACS Nano 13(11):13015–13026

Tortorella S, Karagiannis TC (2014) Transferrin receptor-mediated endocytosis: a useful target for cancer therapy. J Membr Biol 247(4):291–307

Walther W, Minow T, Martin R, Fichtner I, Schlag PM et al (2006) Uptake, biodistribution, and time course of naked plasmid DNA trafficking after intratumoral in vivo jet injection. Hum Gene Ther 17(6):611–624

Wang JP, Hielscher A (2017) Fibronectin: how its aberrant expression in tumors may improve therapeutic targeting. J Cancer 8(4):674–682

Waykar RG, Pawbake AS, Kulkarni RR, Jadhavar AA, Funde AM et al (2016) Influence of RF power on structural, morphology, electrical, composition and optical properties of Al-doped ZnO films deposited by RF magnetron sputtering. J Mater Sci: Mater Electron 27:1134–1143

Yang NJ, Hinner MJ (2015) Getting across the cell membrane: an overview for small molecules, peptides, and proteins. Methods Mol Biol 1266:29–53

Yetisgin AA, Cetinel S, Zuvin M, Kosar A, Kultu O (2020) Therapeutic nanoparticles and their targeted delivery application. Molecules 25:2193

Yu M, Zheng J (2015) Clearance pathways and tumor targeting of imaging nanoparticles. ACS Nano 9(7):6655–6674

Zhang S, Li J, Lykotrafitis G, Bao G, Suresh S (2009) Size-dependent endocytosis of nanoparticles. Adv Mater 21:419–424

Zhou HX, Pang X (2018) electrostatic interactions in protein structure, folding, binding, and condensation. Chem Rev 118(4):1691–1741